



Title	PITHD1 is a proteasome-interacting protein essential for male fertilization
Author(s)	Kondo, Hiroyuki; Matsumura, Takafumi; Kaneko, Mari et al.
Citation	Journal of Biological Chemistry. 2020, 295(6), p. 1658-1672
Version Type	VoR
URL	https://hdl.handle.net/11094/78549
rights	© 2020 ASBMB. Currently published by Elsevier Inc; originally published by American Society for Biochemistry and Molecular Biology. This article is licensed under a Creative Commons Attribution 4.0 International License.
Note	


The University of Osaka Institutional Knowledge Archive : OUKA

<https://ir.library.osaka-u.ac.jp/>

The University of Osaka

PITHD1 is a proteasome-interacting protein essential for male fertilization

Received for publication, September 18, 2019, and in revised form, December 23, 2019. Published, Papers in Press, January 8, 2020, DOI 10.1074/jbc.RA119.011144

Hiroyuki Kondo^{†1},  Takafumi Matsumura^{§¶1}, Mari Kaneko^{||}, Kenichi Inoue^{||}, Hidetaka Kosako^{**},  Masahito Ikawa[§], Yousuke Takahama^{††}, and Izumi Ohigashi^{‡2}

From the [†]Division of Experimental Immunology, Institute of Advanced Medical Sciences, Tokushima University, Tokushima 770-8503, Japan, the [§]Department of Experimental Genome Research, Research Institute for Microbial Diseases, Osaka University, Osaka 565-0871, Japan, the ^{||}Laboratory for Animal Resources and Genetic Engineering, RIKEN Center for Biosystems Dynamics Research, Kobe 650-0047, Japan, the ^{**}Division of Cell Signaling, Fujii Memorial Institute of Medical Sciences, Institute of Advanced Medical Sciences, Tokushima University, Tokushima 770-8503, Japan, the ^{††}Experimental Immunology Branch, National Cancer Institute, National Institutes of Health, Bethesda, Maryland 20892, and the [‡]Laboratory of Biopharmaceutical and Regenerative Sciences, Institute of Molecular Medicine and Life Science, Yokohama City University Association of Medical Science, Yokohama 236-0004, Japan

Edited by George N. DeMartino

The proteasome is a protein-degrading molecular complex that is necessary for protein homeostasis and various biological functions, including cell cycle regulation, signal transduction, and immune response. Proteasome activity is finely regulated by a variety of proteasome-interacting molecules. PITHD1 is a recently described molecule that has a domain putatively capable of interacting with the proteasome. However, it is unknown whether PITHD1 can actually bind to proteasomes and what it does *in vivo*. Here we report that PITHD1 is detected specifically in the spermatids in the testis and the cortical thymic epithelium in the thymus. Interestingly, PITHD1 associates with immunoproteasomes in the testis, but not with thymoproteasomes in the thymus. Mice deficient in PITHD1 exhibit severe male infertility accompanied with morphological abnormalities and impaired motility of spermatozoa. Furthermore, PITHD1 deficiency reduces proteasome activity in the testis and alters the amount of proteins that are important for fertilization capability by the sperm. However, the PITHD1-deficient mice demonstrate no detectable defects in the thymus, including T cell development. Collectively, our results identify PITHD1 as a proteasome-interacting protein that plays a nonredundant role in the male reproductive system.

Protein degradation is a crucial process in cellular homeostasis. The proteasome is a large enzyme complex responsible for protein degradation in cells (1). In most cases, proteasome-dependent proteolysis targets ubiquitinated proteins (2, 3). Protein degradation by the proteasome is important for not only

the maintenance of protein homeostasis, but also various biological functions, including cell cycle regulation, signal transduction, and immune response (3, 4). The proteasome consists of a 20S catalytic core proteasome and regulatory particles that bind to the core proteasome (5). The 20S proteasome is composed of 28 subunits, namely, 2 sets of 7 different α subunits ($\alpha 1$ – $\alpha 7$) and 7 different β subunits ($\beta 1$ – $\beta 7$). Among the 20S proteasome components, $\beta 1$, $\beta 2$, and $\beta 5$ have catalytic activities (6). The proteasome containing $\beta 1$, $\beta 2$, and $\beta 5$ is called the constitutive proteasome and expressed in most tissues. On the other hand, antigen-presenting immune cells, hematopoietic cells, and cells exposed to proinflammatory cytokines express the immunoproteasome in which $\beta 1i$, $\beta 2i$, and $\beta 5i$ are incorporated in place of $\beta 1$, $\beta 2$, and $\beta 5$, respectively (7). Immunoproteasomes possess altered proteolytic activity and participate in the efficient processing of major histocompatibility complex class I-restricted antigens (8). In the thymus, another catalytic subunit $\beta 5t$ is specifically expressed in cortical thymic epithelial cells (cTECs)³ and incorporated into the 20S proteasome together with $\beta 1i$ and $\beta 2i$, thereby forming the thymoproteasome (9, 10). Thymoproteasomes in cTECs are essential for the production of self-antigens that induce the positive selection of CD8⁺ T cells (9, 11). Thymoproteasome-dependent positive selection in the thymus also fine-tunes antigen responsiveness of CD8⁺ T cells in the periphery (12).

The function of the 20S proteasome is modulated by interactions with regulatory proteins. A wide variety of proteasome-interacting proteins have been identified, the most well-known of which is the 19S regulatory particle that binds to both ends of the 20S proteasome to form the 26S proteasome complex (10, 13, 14). The 19S regulatory particle consists of 6 ATPase subunits and 13 non-ATPase subunits, and pre-processes sub-

This work was supported by grants from MEXT-JSPS 17K08884 (to I. O.) and 16H02630 (to Y. T.), Takeda Science Foundation, Sumitomo Foundation, and Novartis Foundation for the Promotion of Science (to I. O.), and the Intramural Research Program of the National Institutes of Health, the National Cancer Institute, and the Center for Cancer Research (to Y. T.). The authors declare that they have no conflicts of interest with the contents of this article. The content is solely the responsibility of the authors and does not necessarily represent the official views of the National Institutes of Health.

This article contains Figs. S1 and S2 and Table S1.

¹ Both authors contributed equally to this work.

² To whom correspondence should be addressed. Tel.: 81-88-633-9475; E-mail: ohigashi@genome.tokushima-u.ac.jp.

³ The abbreviations used are: cTEC, cortical thymic epithelial cell; PITH, proteasome-interacting thioredoxin; mTEC, medullary thymic epithelial cell; tdTomato, tandem dimeric tomato fluorescent protein; DP, double positive; VAP, average path velocity; VCL, curvilinear velocity; VSL, straight-line velocity; TMT, tandem mass tag; PI, propidium iodide; FDR, false discovery rate; gRNA, guide RNA; DAPI, 4',6-diamidino-2-phenylindole; ACN, acetonitrile; GAPDH, glyceraldehyde-3-phosphate dehydrogenase.

This is an Open Access article under the CC BY license.

1658 J. Biol. Chem. (2020) 295(6) 1658–1672

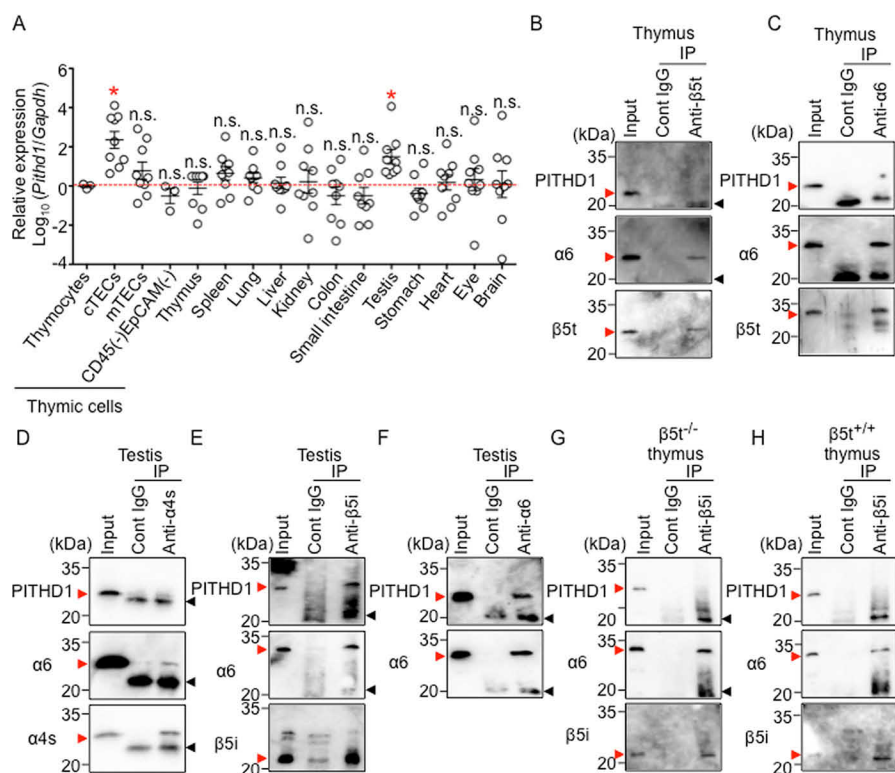


Figure 1. Association capability of PITHD1 with proteasomes in thymus and testis. A, relative mRNA expression of *Pithd1* in the indicated cells and organs isolated from 2-week-old C57BL/6 mice. The expression levels (mean \pm S.E.) of *Pithd1* measured by quantitative RT-PCR were normalized to that of *Gapdh* and compared with the level measured in thymocytes. *, $p < 0.05$, n.s., not significant. Plotted are the results of three independent experiments using samples obtained from three to nine mice. B and C, thymus lysates were immunoprecipitated with anti- β 5t antibody (B), anti- α 6 antibody (C), or control IgG followed by immunoblotting with anti-PITHD1, anti- β 5t, and anti- α 6 antibodies. D–F, testis lysates were immunoprecipitated with anti- α 4s antibody (D), anti- β 5i antibody (E), anti- α 6 antibody (F), or control IgG followed by immunoblotting with anti-PITHD1, anti- α 4s, anti- β 5i, and anti- α 6 antibodies. G and H, thymus lysates from β 5t-deficient (G) or β 5t-sufficient (H) mice were immunoprecipitated with anti- β 5i antibody or control IgG followed by immunoblotting with anti-PITHD1, anti- β 5i, and anti- α 6 antibodies. Red arrowheads indicate each protein. Black arrowheads indicate IgG light chain. All images in panels B–H are representative results of three independent experiments.

strates for degradation by the 20S proteasome. Furthermore, ubiquitin chain-binding receptors, de-ubiquitinating enzymes, and E3 ubiquitin ligases associate with the 19S regulatory particle, and assist or modulate proteasomal functions (13, 15). In addition to the 19S regulatory particle, proteasome activators and inhibitors, such as PA200, PA28, and PI31, directly bind to the 20S proteasome (13–16).

In the course of our explorative study for thymoproteasome modulators in cTECs, we noticed that a functionally unidentified gene encoding PITHD1 was abundantly expressed in cTECs. PITHD1 has a putative proteasome-interacting thioredoxin (PITH) domain that potentially binds to the proteasome. Another PITH domain-containing protein, thioredoxin-like protein 1 (TXNLI), possesses redox activity (17). Unlike TXNLI, PITHD1 lacks redox activity due to the absence of the active-site motif of thioredoxin (18). It has been reported that the ectopic expression of PITHD1 in human leukemia cell lines promotes megakaryocyte development by regulating the expression of RUNX1, a transcription factor that is important for lineage determination between megakaryocytes and erythrocytes in hematopoiesis (18, 19). However, whether PITHD1 can actually bind to proteasomes and what it does *in vivo* are not known. We report herein that PITHD1 is highly expressed in cTECs and the testis. PITHD1 associates with immunoproteasomes in the testis, but not with thymoproteasomes in cTECs.

By producing mice deficient in PITHD1, we show that PITHD1 deficiency causes infertility accompanied with morphological abnormalities and impaired motility of spermatozoa, without detectable defects in the development and function of cTECs. We further show that PITHD1 deficiency reduces proteasome activity in the testis and alters the amount of several proteins that are important for fertilization capability by the sperm. Our study reveals a novel and nonredundant function of PITHD1 as a proteasome-interacting protein essential for the male reproductive system.

Results

Detection of PITHD1 in cTECs and testis

We have previously reported that the β 5t-containing thymoproteasome specifically expressed in cTECs is important for the positive selection of CD8⁺ T cells in the thymus (9–12). Accordingly, we explored proteasome-interacting proteins that could affect the function of thymoproteasomes in cTECs. We found that *Pithd1*, which encodes PITHD1 that contains a putative proteasome-interacting domain, was highly expressed in cTECs in the transcriptomic profiles of thymic epithelial cells (20). Quantitative RT-PCR analysis confirmed that the expression of *Pithd1* was higher in cTECs than other thymic cells, including medullary thymic epithe-

PITHD1 is essential for male fertilization

lial cells (mTECs), CD45⁺ thymocytes, and non-TEC stroma cells (Fig. 1A). Moreover, we detected a significantly higher expression of *Pithd1* in the testis than other organs (Fig. 1A). Thus, we found that *Pithd1* is specifically and abundantly expressed in cTECs and the testis.

The detected PCR products of *Pithd1* were 328 bp in size, derived from spliced RNA, and not 9558 bp from genomic DNA (Fig. S1A). PCR detection of *Hprt* reconfirmed that the amplified signals in our RT-PCR analysis were primarily 249 bp derived from spliced RNAs and not 1087 bp derived from genomic DNAs contaminated in the total RNA samples (Fig. S1A).

PITHD1 associates with immunoproteasomes in testis but not with thymoproteasomes in cTECs

We next examined the association capability of PITHD1 proteins with proteasomes in cTECs and the testis. Immunoprecipitation of mouse thymus lysates using antibody specific for the cTEC-specific thymoproteasome component $\beta 5t$ showed that PITHD1 protein was absent from the precipitates (Fig. 1B). This was not due to the failure of immunoprecipitation by anti- $\beta 5t$ antibody because in addition to $\beta 5t$ protein, $\alpha 6$ protein, which is a 20S proteasome component, was immunoprecipitated by this antibody (Fig. 1B). Similarly, PITHD1 protein in the thymus was not immunoprecipitated by anti- $\alpha 6$ antibody, whereas $\beta 5t$ protein was co-precipitated by the same anti- $\alpha 6$ antibody (Fig. 1C and Fig. S1B). In the testis, the expression of immunoproteasomes and testis-specific proteasomes has been reported (21–23). In the testis-specific proteasome, the $\alpha 4s$ subunit is incorporated into the constitutive proteasome in place of the $\alpha 4$ subunit (21). Immunoprecipitation of testis lysates using antibody specific for $\alpha 4s$ showed the absence of PITHD1 protein in the precipitates (Fig. 1D). Again, this was not due to the failure of immunoprecipitation by anti- $\alpha 4s$ antibody, because in addition to $\alpha 4s$ protein, $\alpha 6$ protein was immunoprecipitated by this antibody (Fig. 1D). On the contrary, immunoprecipitation by anti- $\beta 5i$ antibody or anti- $\alpha 6$ antibody revealed the presence of PITHD1 protein in the precipitates (Fig. 1, E and F). Therefore, these results indicate that PITHD1 associates with $\beta 5i$ -containing immunoproteasomes in the testis either directly or indirectly, whereas it is incapable of binding to $\alpha 4s$ -containing testis-specific proteasomes in the testis or $\beta 5t$ -containing cTEC-specific thymoproteasomes in the thymus.

In $\beta 5t$ -deficient cTECs, $\beta 5i$ is compensatively expressed, thereby forming immunoproteasomes instead of thymoproteasomes (11). Therefore, we examined whether PITHD1 could associate with immunoproteasomes in $\beta 5t$ -deficient cTECs or $\beta 5t$ -sufficient cTECs. We found that immunoprecipitation of $\beta 5t$ -deficient thymus lysates using antibody specific for $\beta 5i$ showed that PITHD1 protein was absent from the precipitates (Fig. 1, G and H). These results indicate that PITHD1 is incapable of binding to thymoproteasomes or immunoproteasomes expressed in cTECs.

Generation of PITHD1-deficient mice

To investigate the physiological role of PITHD1, we next generated PITHD1-deficient mice by introducing a targeting

vector that contained a gene encoding the tandem dimeric tomato fluorescent protein (tdTomato) at the translation initiation site in exon 1 of the *Pithd1* gene along with neighboring genomic sequences into HK3i embryonic stem cells for homologous recombination (Fig. 2A). Thus, the tdTomato fluorescent protein would be detectable in the cells where *Pithd1* was transcribed in this mouse. PCR analysis, Southern blot analysis, and sequencing analysis of genomic DNA isolated from the offspring mice indicated successful germline recombination at the *Pithd1* locus (Fig. 2, B and C). Quantitative RT-PCR analysis showed that *Pithd1* mRNA expression in the thymus and the testis was lost in PITHD1^{−/−} mice (Fig. 2D). Immunoblot analysis also confirmed the loss of PITHD1 protein in the thymus and the testis in PITHD1^{−/−} mice (Fig. 2E). The tdTomato fluorescent protein was detectable in the Ly51-expressing cortical region of the PITHD1^{+/−} thymus (Fig. 2F). Flow cytometric analysis of thymic cells showed tdTomato expression in ~3% of cTECs (Fig. 2G), suggesting that PITHD1 is expressed in a minor subpopulation of cTECs. Intense tdTomato fluorescence was detected in the testicular regions surrounding the lumen of seminiferous tubules (Fig. 2H). Flow cytometric analysis showed that 37% of testicular cells highly expressed the tdTomato fluorescent protein (Fig. 2I). Microscopic inspection of testicular cells revealed that the tdTomato fluorescence was detectable in the cytoplasm of elongated spermatids, whereas it was not detected in round spermatids or other testicular cells (Fig. 2J). The tdTomato fluorescence was also detectable in the cytoplasmic droplets of sperm where proteins are transiently stored and eventually removed in mature sperm (Fig. 2J). We obtained two independent mouse lines exhibiting an identical phenotype, and will show the results from one PITHD1^{−/−} mouse line in this report.

No abnormalities in development and function of cTECs in PITHD1-deficient mice

We then examined the impact of PITHD1 deficiency in the thymus. Hematoxylin and eosin staining and immunofluorescence analysis of the thymic sections showed unaffected cortico-medullary architectures in PITHD1^{−/−} mice (Fig. 3, A and B). Similar to the WT thymus, the cortical regions of PITHD1^{−/−} mice were enriched with $\beta 5t^+$ cTECs and the PITHD1^{−/−} thymic medullas contained Aire⁺ mTECs essential for the generation of self-tolerant T cells (Fig. 3B). Flow cytometric analysis of liberase-digested thymic cells showed that the cellularity of CD45[−]EpCAM⁺UEA1[−]Ly51⁺ cTECs and CD45[−]EpCAM⁺UEA1⁺Ly51[−] mTECs, and their proteasome activity were undisturbed in PITHD1^{−/−} mice (Fig. 3, C and D). Furthermore, neither the development nor the cellularity of thymocytes, including CD4/CD8 subpopulations and CD25/CD44 CD4[−]CD8[−] double-negative subpopulations, was altered by PITHD1 deficiency (Fig. 3, E and F). The development of CD4⁺CD8⁺ double-positive (DP) thymocytes has been subdivided into three subpopulations: CD69[−]TCR β ^{low} pre-selected DP cells (population I), CD69⁺TCR β ^{low} post-selected DP cells (population II), and CD69⁺TCR β ^{high} post-selected DP cells (population III) (24). The cellularity of DP thymocytes in each subpopulation was comparable between WT mice and PITHD1^{−/−} mice (Fig. 3G). Consistent with the normal thymo-

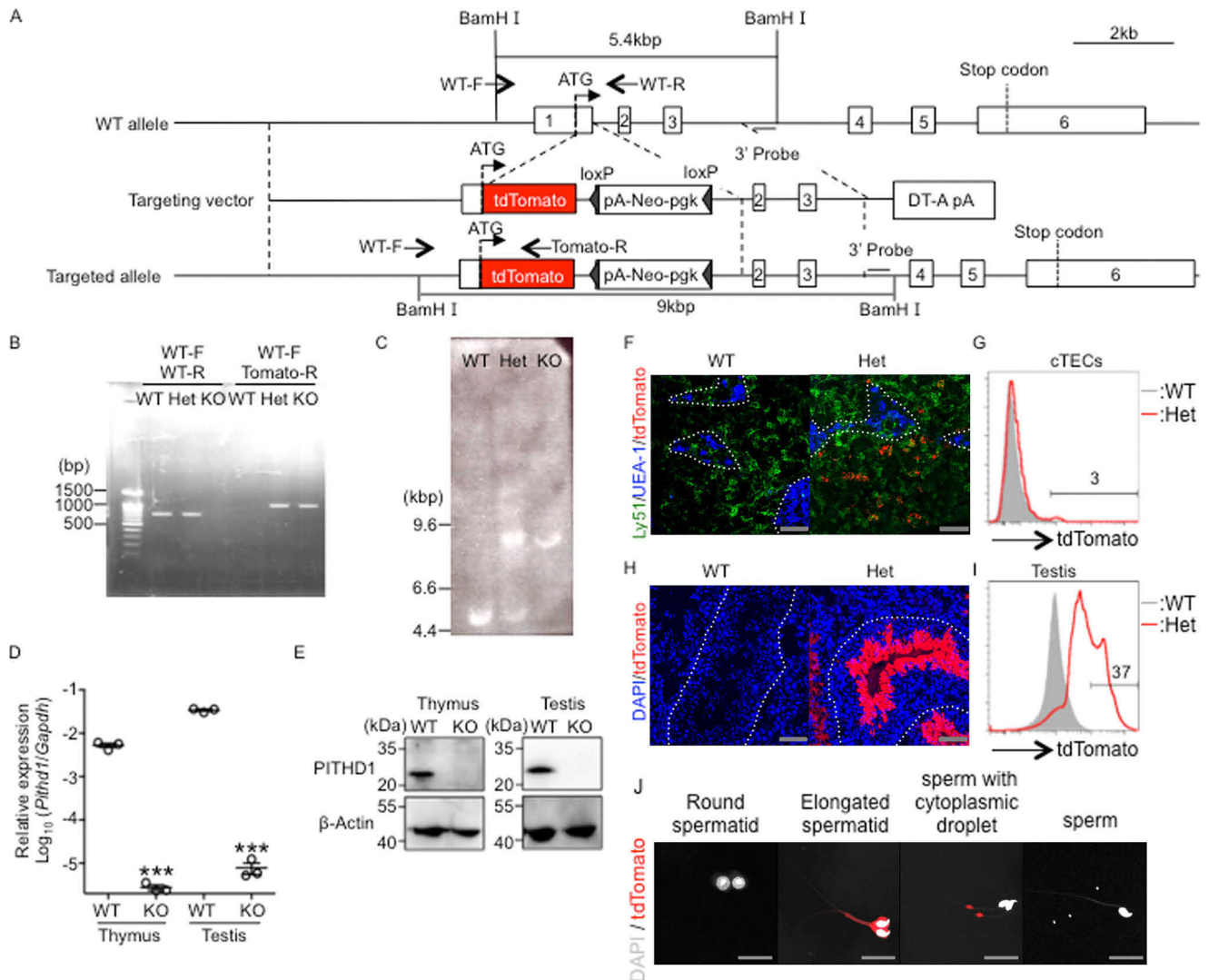


Figure 2. Generation of PITHD1-deficient mice. *A*, schematic diagram of *Pithd1* locus, targeting vector, and targeted allele. *DT-A*, diphtheria toxin. *pgk-Neo-pA*, phosphoglycerate kinase I promoter-driven neomycin resistance gene followed by polyadenylation signal sequence. The 3' probe is for Southern blot analysis. Arrows indicate primers for genotyping PCR. *B*, genotyping PCR analysis of genomic DNA from the indicated mice. Gel electrophoresis of amplified WT allele fragment (763 bp) and targeted allele fragment (1058 bp). Positions of the primers are shown in *A*. WT, PITHD1^{+/+} mice; Het, PITHD1^{+/-} mice; KO, PITHD1^{-/-} mice. *C*, Southern blot analysis of BamHI-digested genomic DNA from the indicated mice. Probe is shown in *A*. Signals at 5.4 and 9 kbp indicate WT and targeted alleles, respectively. *D*, relative mRNA expression of *Pithd1* in thymus and testis isolated from 4-week-old mice. The expression levels (mean \pm S.E.) of *Pithd1* measured by quantitative RT-PCR were normalized to that of *Gapdh*. *E*, immunoblot analysis of PITHD1 protein in thymus and testis isolated from 4-week-old mice. β -Actin was examined as loading control. *F*, immunofluorescence analysis of *tdTomato* (red), Ly51 (green), and UEA1 (blue) in thymic section of PITHD1^{+/+} (PITHD1^{+/tdTomato}) mice. Bar, 100 μ m. *G*, detection of *tdTomato* fluorescence in cTECs analyzed by flow cytometry. *H*, immunofluorescence analysis of *tdTomato* (red) and DAPI (blue) in the testis section. Bar, 100 μ m. *I*, detection of *tdTomato* fluorescence in testicular cells analyzed by flow cytometry. *J*, immunofluorescence analysis of *tdTomato* (red) and DAPI (gray) in the indicated cells isolated from PITHD1^{+/+} (PITHD1^{+/tdTomato}) mice at 8-week-old. Scale bars, 20 μ m. All images (*B*, *C*, *E*, *F*, *H*, and *J*) and histograms (*G* and *I*) are representative results of at least three independent experiments.

cyte development in PITHD1^{-/-} thymus, the cellularity of splenic CD4⁺ T cells and CD8⁺ T cells was comparable with those in WT mice (Fig. 3H). Therefore, these results indicate that despite the physiological expression of PITHD1 in cTECs, PITHD1 deficiency has no detectable impact on the development and function of the thymus.

We also examined whether PITHD deficiency induces the phenotypic alteration of the thymus in β 5t^{-/-} mice. The cellularity of cTECs and mTECs in β 5t^{-/-} mice was not altered by PITHD1 deficiency (Fig. 4A). Furthermore, the cellularity of TCR β ^{high} CD4⁻CD8⁺ thymocytes and splenic CD8⁺ T cells, which was reduced in β 5t^{-/-} mice, was neither further decreased nor recovered by PITHD1 deficiency (Fig. 4, B and

C). Taken together with the finding that PITHD1 is incapable of binding to thymoproteasomes in β 5t-sufficient cTECs or immunoproteasomes in β 5t-deficient cTECs, these results indicate that PITHD1 plays no apparent roles in the thymus in the presence or absence of the thymoproteasome.

PITHD1-deficient mice exhibit male infertility

We then examined the functional significance of PITHD1 in the testis. The weights of the testis and the epididymis were comparable between PITHD1^{+/+} and PITHD1^{-/-} mice (Fig. 5A). The morphology of the testis and the epididymis was undisturbed by PITHD1 deficiency (Fig. 5B). However, when PITHD1^{-/-} male mice were mated with C57BL/6 female mice

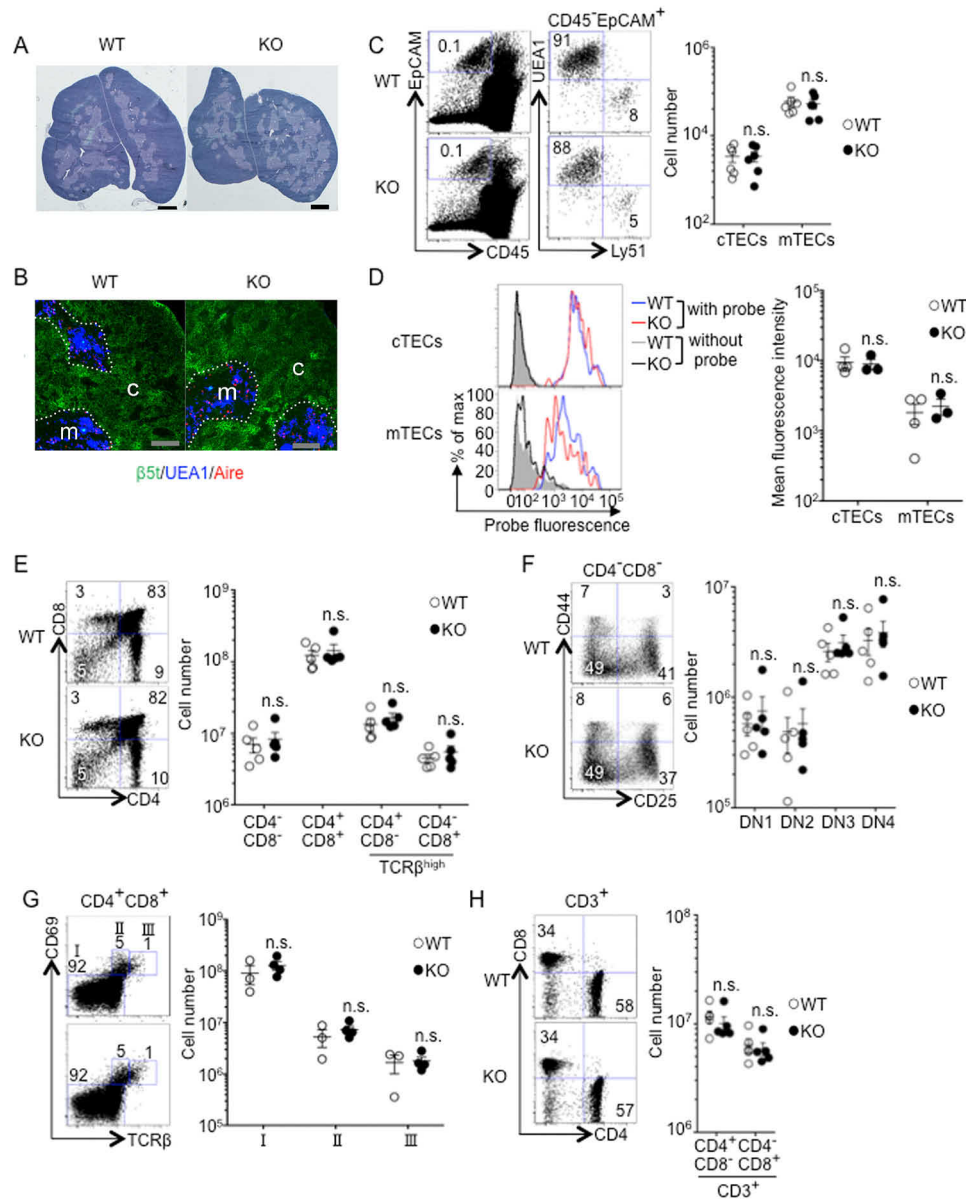


Figure 3. Characterization of the thymus in PITHD1-deficient mice. *A*, hematoxylin and eosin staining of thymic sections from 4-week-old mice. Representative data from three independent mice analyzed in three independent experiments are shown. Scale bar, 500 μ m. *B*, immunofluorescence analysis of β 5t (green), Aire (red), and UEA-1-binding molecules (blue) in thymic sections from 4-week-old mice. Representative data from three independent mice analyzed in three independent experiments are shown. Scale bars, 100 μ m. *C*, flow cytometric analysis of liberase-digested thymic cells isolated from 4-week-old mice. Shown are dot plots of EpCAM and CD45 expression in total cells (left) and UEA1 reactivity and Ly51 expression in CD45⁺EpCAM⁺-gated epithelial cells (right). Plots on the right show cell number (mean \pm S.E.) of CD45⁺EpCAM⁺UEA1⁺Ly51⁺ cTECs and CD45⁺EpCAM⁺UEA1⁺Ly51⁺ mTECs in individual mice, measured in six independent experiments. *D*, histograms show the detection of proteasome activity by cell-permeable triple-leucine substrate-based fluorescent probe in cTECs and mTECs of PITHD1^{+/+} mice (blue line) and PITHD1^{-/-} mice (red line). Shaded area and black line represent background fluorescence profiles without the addition of proteasome probe in PITHD1^{+/+} TECS and PITHD1^{-/-} TECS, respectively. Plots on the right show mean fluorescence intensity (mean \pm S.E.) of indicated cells in individual mice, measured in three independent experiments. *E*, flow cytometric analysis of total thymocytes isolated from 4-week-old mice. Shown are dot plots of CD4 and CD8 expression in propidium iodide⁺ (PI⁺) thymocytes. Plots on the right show cell number (mean \pm S.E.) of indicated cell populations in individual mice, measured in five independent experiments. *F*, flow cytometric analysis of CD44 and CD25 expression in CD4⁺CD8⁺ thymocytes. Plots on the right show cell number (mean \pm S.E.) of CD44⁺CD25⁺ cells (DN1), CD44⁺CD25⁺ cells (DN2), CD44⁺CD25⁺ cells (DN3), and CD44⁺CD25⁺ cells (DN4) in individual mice, measured in five independent experiments. *G*, flow cytometric analysis of CD69 and TCR β expression in CD4⁺CD8⁺ thymocytes. Plots on the right show cell number (mean \pm S.E.) of CD69⁺TCR β ^{low} cells (population I), CD69⁺TCR β ^{low} cells (population II), and CD69⁺TCR β ^{high} cells (population III) in individual mice, measured in three independent experiments. *H*, flow cytometric analysis of spleen cells. Shown are dot plots of CD4 and CD8 expression in CD3⁺ splenic T cells. Plots on the right show cell number (mean \pm S.E.) of indicated cell populations in individual mice, measured in five independent experiments. Numbers in dot plots indicate frequency of cells within indicated area. n.s., not significant.

for 2 months, no pregnancy was observed in female mice even though vaginal plug formation was detectable (Fig. 5C). On the other hand, PITHD1^{+/+} male mice were able to impregnate female mice and 7 pups were produced on average per pregnancy (Fig. 5C). An *in vitro* fertilization assay confirmed the

fertilization incapability of sperm isolated from PITHD1^{-/-} mice in both cumulus-intact and cumulus-free conditions (Fig. 5D). However, PITHD1^{-/-} sperm were able to fertilize an egg under the zona pellucida-free condition (Fig. 5D). Therefore, these results indicate that sperm from PITHD1^{-/-} mice are

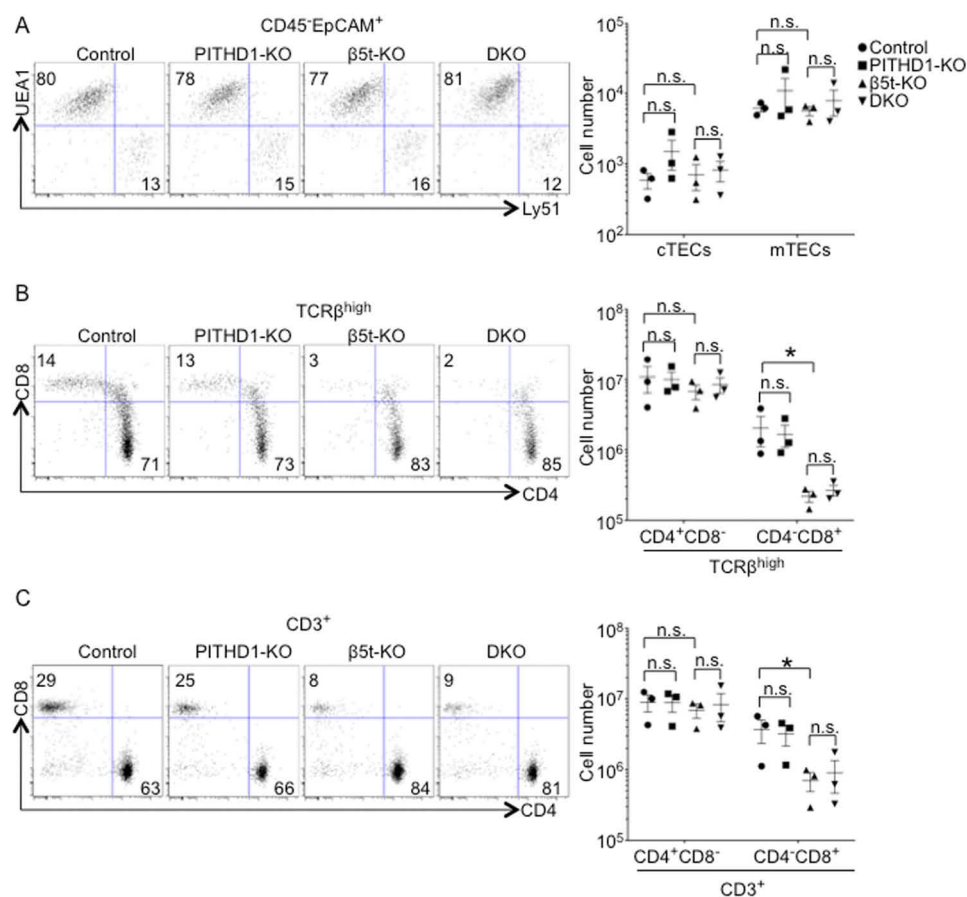


Figure 4. T cell development in $\beta 5t$ /PITHD1 double-deficient mice. A, flow cytometric analysis of liberase-digested thymic cells from the indicated mice. Shown are dot plots of UEA1 reactivity and Ly51 expression in CD45⁺EpCAM⁺-gated epithelial cells. Plots on the right show cell number (mean \pm S.E.) of CD45⁺EpCAM⁺UEA1⁺Ly51⁺ cTECs and CD45⁺EpCAM⁺UEA1⁺Ly51⁺ mTECs in individual mice, measured in three independent experiments. B, flow cytometric analysis of total thymocytes. Shown are dot plots of CD4 and CD8 expression in TCR^{high} thymocytes. Plots on the right show cell number (mean \pm S.E.) of indicated cell populations in individual mice, measured in three independent experiments. C, flow cytometric analysis of spleen cells. Shown are dot plots of CD4 and CD8 expression in CD3⁺ splenic T cells. Plots on the right show cell number (mean \pm S.E.) of the indicated cell populations in individual mice, measured in three independent experiments. Numbers in dot plots indicate frequency of cells within indicated area. *, $p < 0.05$; n.s., not significant.

defective in fertilization capability due to passage disability through egg layers such as cumulus and zona pellucida. We noticed no defects in the fertility of female PITHD1^{-/-} mice (data not shown).

PITHD1-deletion mice exhibit similar phenotype to PITHD1-deficient mice

The results so far indicated that PITHD1 is important for male reproductive function rather than cTEC function. However, it remained possible that the artificial expression of tdTomato in PITHD1^{-/-} mice might have hindered the phenotypes that could have resulted simply from the loss of PITHD1. Therefore, we next generated a new set of PITHD1-deletion mice (Δ/Δ) in that the genomic region spanning the middle of exon 1 to exon 3 was deleted by CRISPR/Cas9 technology (Fig. 6A). PCR analysis of genomic DNA isolated from the offspring mice indicated successful deletion of the *Pithd1* genomic sequence (Fig. 6B). Quantitative RT-PCR analysis and immunoblot analysis confirmed the loss of PITHD1 at mRNA and protein levels (Fig. 6, C and D). Like PITHD1^{-/-} mice, the cellularity of Ly51⁺ cTECs and UEA1⁺ mTECs as well as those of thymocyte subpopulations and splenic T cells was undisturbed in PITHD1 Δ/Δ mice (Fig. 6, E–G). The morphology of the testis and the epididymis

was also undisturbed in PITHD1 Δ/Δ mice (Fig. 6H). However, an *in vitro* fertilization assay of sperm isolated from PITHD1 Δ/Δ mice revealed fertilization incapability in both cumulus-intact and cumulus-free conditions, like PITHD1^{-/-} mice and unlike PITHD1^{WT/ Δ} mice (Fig. 6I). Therefore, these results indicate that the aberrant expression of the tdTomato fluorescent protein has essentially no impact on the phenotype of PITHD1^{-/-} mice, and reinforce that the impaired fertilization capability of sperm is caused by PITHD1 deficiency.

PITHD1 deficiency results in abnormal morphology and impaired motility of sperm

To understand the mechanism behind male infertility caused by PITHD1 deficiency, we next examined the morphology of mature sperm isolated from the cauda epididymis of PITHD1^{-/-} mice (Fig. 7A). The number of sperm was comparable between PITHD1^{+/+} mice and PITHD1^{-/-} mice (data not shown). However, the frequency of sperm with normal morphology was significantly reduced in PITHD1^{-/-} mice compared with PITHD1^{+/+} mice (Fig. 7B). On the other hand, the frequency of sperm with multiheads was significantly increased in PITHD1^{-/-} mice (Fig. 7B). The reduction of morphologically normal sperm and the increase of sperm with

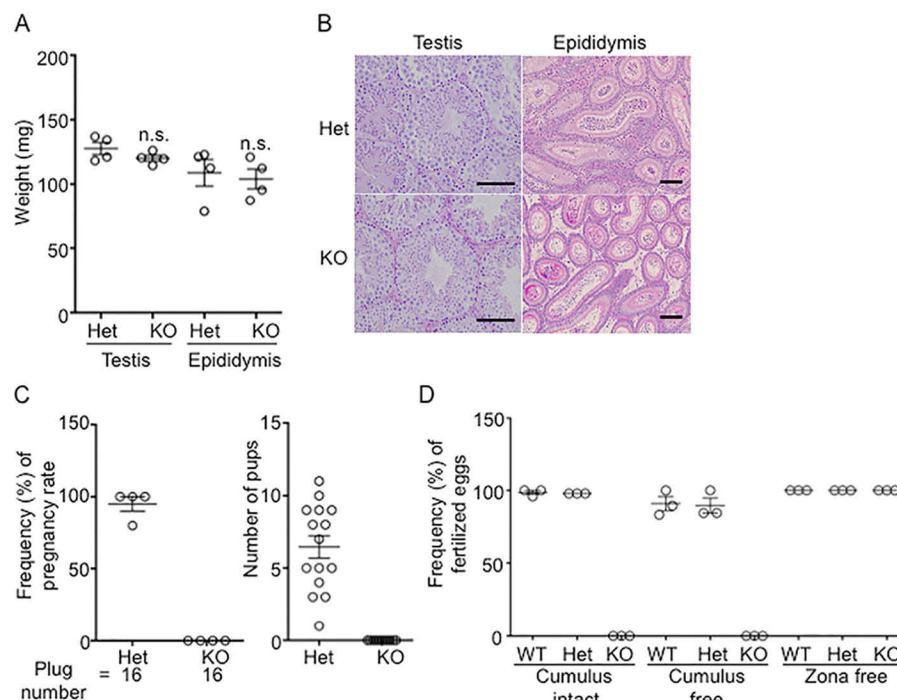


Figure 5. Male infertility in PITHD1-deficient mice. *A*, weights (mean \pm S.E., individually measured for four mice) of testis and epididymis in 8-week-old mice. *n.s.*, not significant. *B*, hematoxylin and eosin staining of testis and epididymis sections from 8-week-old mice. Representative data from three independent mice analyzed in three independent experiments are shown. Scale bar, 100 μ m. *C*, four PITHD1^{+/-} male mice and four PITHD1^{-/-} male mice were mated with C57BL/6 female mice, respectively. Plots on the left show pregnancy rate (pregnancy/vaginal plug formation) in female mice mated with indicated male mice. Plots on the right show the number of pups born in one pregnancy. Mean \pm S.E. are shown by black bars. *D*, *in vitro* fertilization assay. Sperm from indicated male mice were incubated with cumulus-intact, cumulus-free, or zona-free WT eggs, and the numbers of eggs carrying pronuclei (zona-free eggs; $n = 176$) and of eggs that had reached the 2-cell stage (cumulus-intact eggs; $n = 521$, cumulus-free eggs; $n = 247$) were counted. The frequencies (mean \pm S.E.) of fertilized eggs from three independent experiments are plotted.

abnormal midpiece and multiheads were also detected in PITHD1 ^{Δ/Δ} mice (Fig. 7C). We next examined the motility of sperm incubated in TYH medium for 10 min or 2 h by measuring the average path velocity (VAP), the curvilinear velocity (VCL), and the straight-line velocity (VSL). The values of these motility parameters for PITHD1^{+/-} sperm were comparable with those for PITHD1^{+/-} sperm after 10 min incubation (Fig. 7D). However, a significant reduction of these velocities was detected in PITHD1^{-/-} sperm after 2 h incubation (Fig. 7D). Similarly, motility reduction in PITHD1 ^{Δ/Δ} sperm was detected after 2 h incubation (Fig. 7E). Morphological analysis revealed that motile sperm from PITHD1^{+/-} and PITHD1^{WT/ Δ} mice were predominantly morphologically normal, whereas a majority of motile sperm from PITHD1^{-/-} and PITHD1 ^{Δ/Δ} mice exhibited morphological abnormalities (Fig. 7, F and G). Collectively, these results indicate that PITHD1 deficiency causes impaired sperm motility accompanied with morphological abnormalities.

PITHD1 regulates proteasome activity in testicular cells

So far, we have shown that PITHD1 associates with β 5i-containing immunoproteasomes in the testis and that its deficiency causes impaired sperm motility. We therefore speculated the possibility that PITHD1 deficiency might affect proteasome activity in the testis. In mice that carried the *Pithd1* knock-out tdTomato knock-in allele (Fig. 2A), tdTomato fluorescence expression enabled the detection of cells in that *Pithd1* was transcribed. In the testis of these mice, tdTomato fluorescence

was detected in the elongated spermatids and the cytoplasmic droplets of sperm (Fig. 2J). We examined proteasome activity in tdTomato⁺ and tdTomato⁻ cells in the testis by using a cell-permeable triple-leucine substrate-based fluorescent probe that shows high affinity binding to the chymotrypsin-like catalytic site of proteasomes (25). The fluorescence intensity detected with this probe could reflect the chymotrypsin-like activity and/or the abundance of proteasomes. We found that the fluorescence intensity in tdTomato⁺ testicular cells was significantly reduced in PITHD1^{-/-} mice compared with PITHD1^{+/-} mice (Fig. 8, A and B, and Fig. S2A). We also found that the fluorescence intensity was unaltered in tdTomato⁻ testicular cells, tdTomato⁺ sperm, and tdTomato⁻ sperm by PITHD1 deficiency (Fig. 8, A and B). It was possible that the reduced proteasome activity was due to the reduced abundance of proteasomes. Indeed, the amount of the immunoproteasome component β 5i in tdTomato⁺ testicular cells was significantly reduced in PITHD1^{-/-} mice compared with that in PITHD1^{+/-} mice (Fig. S2B). We also found that the proteasome activity measured by the fluorescent probe was higher in tdTomato⁺ testicular cells than tdTomato⁻ testicular cells, and subsequently reduced in tdTomato⁺ sperm and tdTomato⁻ sperm in both PITHD1^{+/-} mice and PITHD1^{-/-} mice (Fig. 8, A and B). Correlated with the higher proteasome activity in tdTomato⁺ testicular cells than sperm, immunoblot analysis using lysate from PITHD1^{+/+} cells showed that the amount of PITHD1 protein was high in the testis but reduced in caput

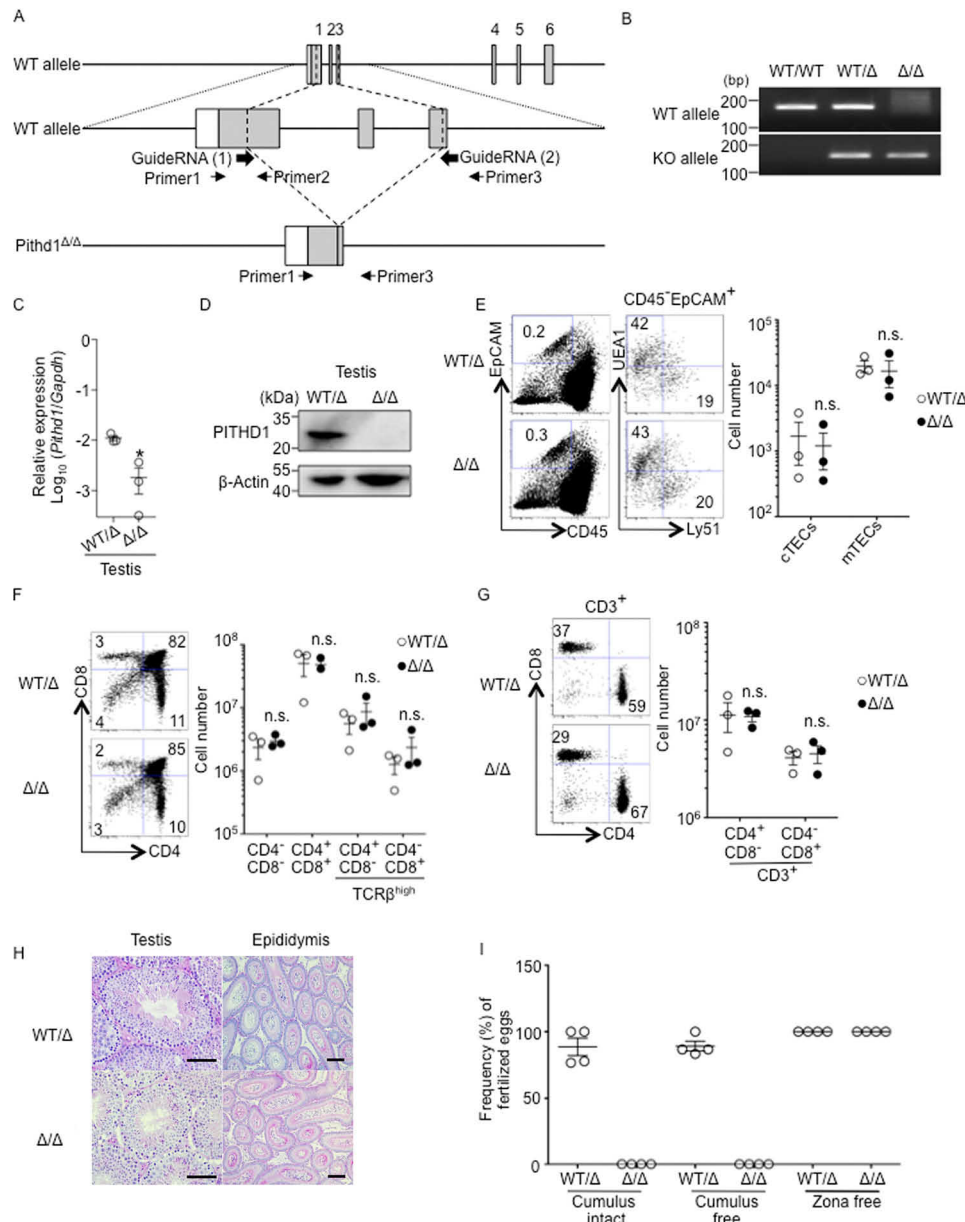


Figure 6. Generation of PITHD1-deletion mice by CRISPR/Cas9 technology. *A*, schematic diagram of *Pithd1* locus and targeted allele. *Bold arrows* indicate the position of guide RNA. Primer 1, Primer 2, and Primer 3 are for genotyping PCR. *B*, genotyping PCR analysis of genomic DNA from indicated mice. Gel electrophoresis of amplified WT allele fragment (198 bp) and targeted allele fragment (167 bp). Positions of the primers are shown in *A*. Representative data from three independent mice analyzed in three independent experiments are shown. *C*, relative mRNA expression of *Pithd1* in testis. The expression levels (mean \pm S.E.) of *Pithd1* measured by quantitative RT-PCR were normalized to that of *Gapdh*. *, $p < 0.05$. Plotted are the results of three independent experiments using three mice per group. *D*, immunoblot analysis of PITHD1 protein in testis isolated from 8-week-old mice. β -Actin was examined as loading control. Representative results of three independent experiments are shown. *E*, flow cytometric analysis of liberase-digested thymic cells isolated from 8-week-old mice. Shown are dot plots of EpCAM and CD45 expression in total cells (left) and UEA1 reactivity and Ly51 expression in CD45⁺EpCAM⁺ epithelial cells (right). Plots on the right show cell number (mean \pm S.E.) of CD45⁺EpCAM⁺ UEA1⁺Ly51⁺ cTECs and CD45⁺EpCAM⁺ UEA1⁺Ly51⁺ mTECs in individual mice, measured in three independent experiments. *F*, flow cytometric analysis of total thymocytes isolated from 8-week-old mice. Shown are dot plots of CD4 and CD8 expression in propidium iodide⁻ (*PI*⁻) thymocytes. Plots on the right show cell number (mean \pm S.E.) of indicated cell populations in individual mice, measured in three independent experiments. *G*, flow cytometric analysis of total spleen cells isolated from 8-week-old mice. Shown are dot plots of CD4 and CD8 expression in CD3⁺ splenic T cells. Plots on the right show cell number (mean \pm S.E.) of indicated cell populations in individual mice, measured in three independent experiments. *Numbers* in dot plots indicate frequency of cells within indicated area. *n.s.*, not significant. *H*, hematoxylin and eosin staining of testis and epididymis sections from 8-week-old mice. Representative data from three independent experiments are shown. Scale bar, 100 μ m. *I*, *in vitro* fertilization assay. Sperm from indicated male mice were incubated with cumulus-intact, cumulus-free, or zona-free WT eggs, and the numbers of eggs carrying pronuclei (zona-free eggs; $n = 177$) and of eggs that had reached the 2-cell stage (cumulus-intact eggs, $n = 101$; cumulus-free eggs; $n = 38$) were counted. The frequencies (mean \pm S.E.) of fertilized eggs from four independent experiments are plotted.

epididymal sperm and cauda epididymal sperm (Fig. 8C). Taken together, these results indicate that PITHD1 regulates proteasome activity including its abundance in testicular cells including elongated spermatids.

We finally performed MS-based quantitative proteomic analysis of sperm isolated from PITHD1^{+/+} mice and PITHD1^{-/-} mice. Proteins extracted from sperm were digested with trypsin, and the peptides were labeled with iso-

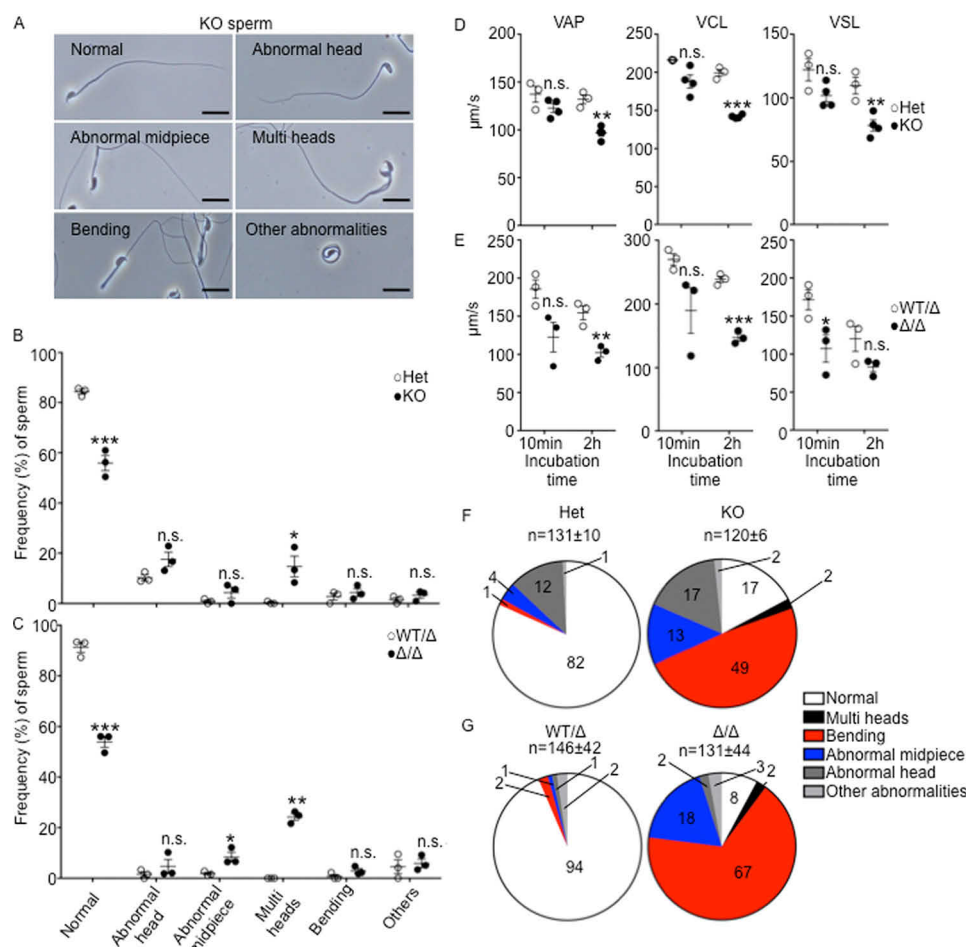


Figure 7. Morphological abnormalities and impaired motility of PITHD1-deficient sperm. A, morphology of sperm isolated from PITHD1^{-/-} mice. All images are representative results of three independent mice in three independent experiments. B and C, frequency (mean \pm S.E.) of sperm exhibiting indicated morphologies, measured individually in PITHD1^{-/-} mice (B), PITHD1 Δ/Δ mice (C), and control mice (three mice per group). *, $p < 0.05$; **, $p < 0.01$; ***, $p < 0.001$; n.s., not significant. D and E, sperm isolated from PITHD1^{-/-} mice (D), PITHD1 Δ/Δ mice (E), and control mice were allowed to swim out from the dissected cauda epididymis in TYH medium for 10 min (noncapacitating) or 2 h (capacitating). VAP, VCL, and VSL were measured using a computer-assisted sperm analysis system. Shown are graphs of each parameter (mean \pm S.E.) measured in sperm isolated individually from three to four mice per group. *, $p < 0.05$; **, $p < 0.01$; ***, $p < 0.001$; n.s., not significant. F and G, frequencies of indicated morphologies observed in motile sperm isolated from PITHD1^{-/-} mice (F), PITHD1 Δ/Δ mice (G), and control mice. n, sperm number measured in individual mice (three mice per group).

baric tandem mass tag (TMT) reagents. A high confidence analysis at 1% false discovery rate (FDR) of LC-tandem mass spectrometric (LC-MS/MS) profiles resulted in the identification and quantification of 3,727 protein species (Table S1). Although few proteins showed significant alteration in abundance ($Q < 0.05$) in the comparison between PITHD1^{+/+} mice and PITHD1^{-/-} mice, modest differences ($Q < 0.15$) in the amounts of several proteins were detected (Fig. 8D). Only one protein MROH7 showed significantly ($Q < 0.15$) higher expression in sperm from PITHD1^{-/-} mice than PITHD1^{+/+} mice, but its role in sperm is unknown (Fig. 8D). On the contrary, seven protein species were detected at significantly ($Q < 0.15$) lower amounts in sperm from PITHD1^{-/-} mice than PITHD1^{+/+} mice (Fig. 8D). Among these seven proteins, ACE, PRKAR1A, and TEX101 are known to be important for the fertilization capability of sperm (26–29). The other four proteins (RPS27A, PRSS39, and the 19S proteasomal regulatory subunits PSMC2 and PSMD1) were also implicated in sperm function (30–34). Therefore, these results suggest that the PITHD1-mediated regulation of proteasomes in testicular cells

including elongated spermatids is required for the quantitative control of proteins important for the fertilization capability of sperm.

Discussion

The present results demonstrate that PITHD1, which is highly expressed in cTECs and the testis, associates with the immunoproteasomes in the testis, but not with $\alpha 4$ s-containing testis-specific proteasomes or cTEC-specific thymoproteasomes. The present results also demonstrate that mice specifically deficient in PITHD1 show male infertility accompanied with morphological abnormalities and impaired motility of sperm. PITHD1 deficiency results in the reduction of proteasome activity and/or abundance in testicular cells including elongated spermatids and the alteration in the amount of proteins important for fertilization capability in sperm. Thus, this study reveals that PITHD1 is a proteasome-interacting protein that plays a nonredundant role in the male reproductive system.

Our proteomic analysis of sperm shows that the amounts of 7 proteins (ACE, PRKAR1A, RPS27A, TEX101, PRSS39, PSMC2,

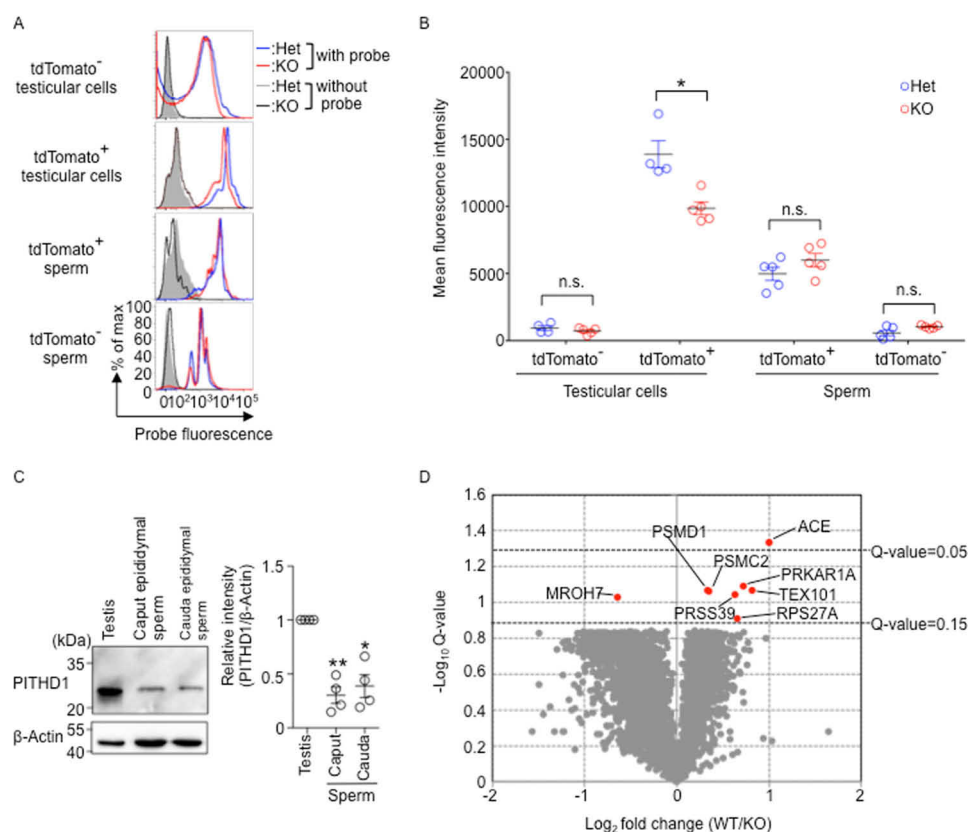


Figure 8. Alteration of proteasome activity in testicular cells by PITHD1 deficiency. A, histograms show the detection of proteasome activity by cell-permeable triple-leucine substrate-based fluorescent probe in testicular cells and sperm of PITHD1^{+/+} mice (blue line) and PITHD1^{-/-} mice (red line). Shaded area and black line represent background fluorescence profiles without the addition of proteasome probe in PITHD1^{+/+} mice and PITHD1^{-/-} mice, respectively. Representative data from four to five independent mice measured in four independent experiments are shown. B, mean fluorescence intensity (mean \pm S.E.) of a triple-leucine substrate-based fluorescent probe in indicated cells in PITHD1^{+/+} mice (blue symbols) and PITHD1^{-/-} mice (red symbols) from four independent experiments. *, $p < 0.05$. C, immunoblot analysis of PITHD1 protein in testis and sperm isolated from cauda epididymis and caput epididymis of PITHD1^{+/+} mice. β -Actin was examined as loading control. Representative results of four independent experiments are shown. Graph shows the intensity (mean \pm S.E.) of PITHD1 signal detected by immunoblotting relative to β -Actin signal. *, $p < 0.05$; **, $p < 0.01$. D, volcano plot analysis of proteomes for sperm isolated from PITHD1^{+/+} mice and PITHD1^{-/-} mice (three mice per group) at 8-week-old. Detected proteins are plotted as log₂-fold changes versus $-\log_{10}$ Q-values.

and PSMD1), which have all been implicated in male fertilization capability, are reduced by PITHD1 deficiency. It was previously reported that mice deficient in ACE and its specific substrate TEX101 exhibit male infertility due to the impaired ability of sperm to migrate into the oviduct (26–28). The haploinsufficiency of PRKAR1A was reported to cause the fertility defects accompanied with morphological abnormalities of sperm in both mouse and human (29). The association between male infertility and the reduced expression of RPS27A and the 19S regulatory subunit PSMC2 was shown in transcriptomic and proteomic analyses of human sperm (30, 31, 33). It was also suggested that PRSS39 and the 19S regulatory subunit PSMD1 play a role in zona penetration by sperm (32, 34). In this study, we demonstrated that the reduction of proteasome activity and/or abundance by PITHD1 deficiency is detectable in testicular cells including elongated spermatids, rather than sperm. It is therefore conceivable that the regulation of proteasomes by PITHD1 in testicular cells is important for the optimal expression of these 7 proteins in mature sperm.

Our results show that the reduction of proteasome activity and/or abundance in testicular cells is modest in PITHD1-deficient mice. It was recently reported that mice deficient in $\alpha 4s$, a component of testis-specific proteasome, exhibit infertility in

male, and proteins that are normally degraded during spermatogenesis are accumulated in testicular cells in $\alpha 4s$ -deficient mice, although the reduction of proteasome activity is also mild in the testis of these mice (22, 23). It was also reported that proteasome activity *per se* is not reduced in $\beta 5t$ -deficient cTECs, although $\beta 5t$ deficiency markedly impairs the positive selection of CD8⁺ T cells in the thymus (9–11, 20). Therefore, the modest reduction of proteasome activity and/or abundance in testicular cells by PITHD1 deficiency may sufficiently affect the function of key proteins that are important for fertilization capability.

Our immunoprecipitation experiments reveal that PITHD1 associates with immunoproteasomes in the testis but not with immunoproteasomes or thymoproteasomes in the thymus. It was previously demonstrated that the proteasome activator PA200 is highly expressed in the testis, and ~90% of proteasomes in the testis contain PA200 at either one or both ends of the 20S proteasomes (35, 36). On the contrary, in our recently published proteomic profiles, PA200 was undetectable in cTECs (20). Therefore, PA200 expression in the testis may support the association of PITHD1 with immunoproteasomes in the testis but not in cTECs. Our results also show that PITHD1 does not associate with $\alpha 4s$ -containing testis-specific protea-

PITHD1 is essential for male fertilization

somes. It was previously reported that the $\alpha 4$ s subunit is highly expressed in spermatocytes and spermatids, and the $\alpha 4$ s-containing testis-specific proteasomes contain PA200 (21–23, 36). However, $\alpha 4$ s is incorporated into the constitutive proteasomes and not the immunoproteasomes (21). It is possible that the type of 20S proteasomes, in addition to the association with other proteasome-interacting proteins, is important for the association of PITHD1 with proteasomes.

The role of proteasome-interacting proteins, including PA200 and PA28 γ , in the male reproductive system was studied previously. PA200 is essential for the acetylation-associated degradation of core histones to replace histones with protamines in elongated spermatids, and that is a necessary chromatin remodeling that gives rise to healthy sperm (36). Indeed, mice deficient in PA200 exhibit male subfertility accompanied with the reduced production of healthy sperm (37). It was also reported that PA28 γ -deficient male mice are subfertile due to the reduced production and motility of sperm (38, 39). Furthermore, PA200/PA28 γ double deficiency causes infertility with defect in sperm motility (40). Therefore, it is possible that PITHD1 functions in the male reproductive system coordinately with other proteasome-interacting proteins, including PA200 and PA28 γ .

We further show that the impaired motility and the morphological abnormalities of sperm are caused by PITHD1 deficiency. The morphological abnormalities of sperm from PITHD1-deficient mice could be the cause of the defect in sperm motility. However, ~50% of sperm showed normal morphology in PITHD1-deficient mice under macroscopic observation. The motility of sperm is generated by axoneme in flagellum, which consists of two central microtubules surrounded by nine pairs of microtubules (41). Therefore, morphologically normal sperm in PITHD1-deficient mice may indeed have a defect in the ultrastructure of flagellum, including microtubules, which is undetectable under macroscopic observation.

Finally, our results show that PITHD1-tdTomato protein is detected in ~3% of cTECs. In the thymus, both cTECs and mTECs consist of diverse subpopulations, and cTECs are heterogeneous in the expression of functionally important molecules, including interleukin-7, delta-like-4, and major histocompatibility complex class II (42). The heterogeneity of cTECs in PITHD1-tdTomato expression newly detected in this study offers an additional diversity in cTECs. Our results also show that PITHD1-deficient mice exhibit no apparent defects in the thymus, including the development of TECs and thymocytes. Our results further denote that the impaired generation of TCR β^{high} CD4 $^{-}$ CD8 $^{+}$ thymocytes in $\beta 5t$ -deficient thymus is neither further decreased nor recovered by PITHD1 deficiency. These results indicate that PITHD1 plays no apparent roles in the thymus in the presence or absence of the thymoproteasome. However, it is still possible that PITHD1 in the thymus plays a presently unknown role mediated by a minor subpopulation of cTECs.

In conclusion, the present study reveals the nonredundant function of the testis-specific proteasome-interacting protein PITHD1 in the male reproductive system in mouse. PITHD1 protein has been detected in the human testis (The Human Protein Atlas public database). Although the association

between PITHD1 and infertility has not been reported in genome-wide association studies, PITHD1 could actually be an additional molecule important in human male fertility. Our findings may provide clues to better understand the molecular mechanisms in the male reproductive system common to mouse and human.

Experimental procedures

Mouse

C57BL/6 mice, B6D2F1 mice, and ICR mice were obtained from SLC. $\beta 5t$ -deficient mice were described previously (9). All mouse experiments were performed with consent from the Animal Experimentation Committee of Tokushima University (T28-58), from the Animal Care and Use Committee of the Research Institute for Microbial Diseases, Osaka University (H28-08, H30-01), and from the Institutional Animal Care and Use Committee (IACUC) of RIKEN Kobe Branch (A2001-03).

Generation of PITHD1-deficient mice

The targeting vector shown in Fig. 2 was prepared by subcloning *PITHD1*-containing mouse genomic DNA and tdTomato-encoding cDNA (Clontech) into a plasmid containing a pgk-neo cassette. The linearized targeting vector was introduced into HK3i ES cells from C57BL/6N embryos (43). Targeted alleles were screened by genomic PCR analysis and Southern blot analysis. PITHD1 $^{-}$ mice (PITHD1 $^{\text{tm1(tdTomato)}}$, accession no. CDB1274K) are available to the scientific community. The primers used for genotyping PCR were as follows: WT-F, 5'-ACGCTTGAACGGTACCACTG-3'; WT-R, 5'-GCTGCGA-ACTCAAAGACCA-3'; tdTomato-R, 5'-GGTCTTGAAC-CCACCAGGT-3'.

Generation of PITHD1-deletion mice

As shown in Fig. 6A, guide RNAs, which recognize sequences in the exon 1 (5'-GCTGTACCTGCGCATCGACC-3') or exon 3 (5'-ACTCACAGTCTCATCTCCGA-3'), were designed using CRISPRdirect web tool. Their cleavage activity was validated by single-strand annealing assay (44). WT zygotes were obtained by mating superovulated B6D2F1 females with B6D2F1 males. The two gRNA/Cas9 complexes were electroporated into two pronuclear zygotes using a super electroporator NEPA21 (NEPA GENE, Chiba, Japan) (45). The zygotes were cultivated in KSOM medium overnight, and the developed two-cell stage embryos were transferred into the oviducts of pseudopregnant ICR females. The F0 pups obtained were genotyped by PCR using primers 1 and 2 for detecting WT allele or primers 1 and 3 for detecting knockout allele. The DNA sequence of the mutant alleles (PITHD1 $^{\Delta}$ or PITHD1 $^{\text{em1}}$) was further confirmed by Sanger sequencing. The crRNA target sequences and primers for genotyping were as follows: Primer-1, 5'-CGCCATGTGCGACGGCCACAG-3'; Primer-2, 5'-GAGCGGTCCGGTCCGCTCCTC-3'; Primer-3, 5'-TAGGTG-GGAGTCTCCCGAGG-3'.

Southern blot analysis

Genomic DNA extracted from the liver was digested with BamHI, electrophoresed in 1% agarose, and transferred to

nylon membrane (Hybond-N⁺, GE Healthcare). Probes were labeled with a PCR DIG Probe Synthesis Kit (Roche), and hybridization was detected using anti-DIG-AP Fab fragment (Roche Applied Science), CDP-STAR (Roche Applied Science), and Light Capture II (Atto). The primers used for Southern blot analysis were as follows: forward, 5'-AGCTTGTCTGTCTCTGTGGA-3'; reverse, 5'-CAGTGTCTGTAAGTCATG-GAGC-3'.

Quantitative RT-PCR analysis

Total cellular RNA was reverse-transcribed (RT) with PrimeScript Reverse Transcriptase (TaKaRa). Quantitative real-time PCR was performed using SYBR Premix Ex Taq (TaKaRa) and a StepOnePlus Real-Time PCR System or a 7900HT Sequence Detection System (Applied Biosystems). The primers used were as follows: *Pithd1*, 5'-CCGTTTACGGGCAATGTCAA-3' and 5'-CATAGTTGCAGATGGTCACC-3'; *Gapdh*, 5'-CCGGTGCTGAGTATGTCGTG-3' and 5'-CAGTCTTC-TGGGTGGCAGTG-3'; *Hprt*, 5'-GCTGGTGAAGGACC-TCT-3' and 5'-CACAGGACTAGAACACCTGC-3'. Amplified products were confirmed to be single bands in gel electrophoresis and normalized to the amount of *Gapdh* amplification products.

Immunoprecipitation

Thymic cells were isolated from newborn mice. Testicular cells were isolated from 6-week-old mice. The cells were lysed in ice-cold lysis buffer containing 0.2% Nonidet P-40, 25 mM Tris-HCl, pH 7.5, 1 mM DTT, 2 mM ATP, and 5 mM MgCl₂, and clarified by centrifugation at 20,000 × *g* for 15 min at 4 °C. For immunoprecipitation, anti-β5t antibody (MBL International) (20), anti-β5i antibody (Proteintech) (46), anti-α4s antibody (Proteintech) (22), or anti-α6 antibody (Bethyl Laboratories) was bound to Protein G-Sepharose beads (GE Healthcare) and mixed with the cell lysates at 4 °C for 2 h. The beads were washed with lysis buffer, and immunoprecipitated molecules were eluted with 2× SDS sample buffer containing 125 mM Tris-HCl, pH 6.5, 4% SDS, 20% glycerol, 0.2 M DTT, and 0.01% bromophenol blue.

Immunoblot analysis

The immunoprecipitated molecules or the cell lysates were boiled with SDS sample buffer, separated by SDS-PAGE, and transferred to a polyvinylidene difluoride membrane. Membranes were probed with anti-PITHD1 antibody (Sigma-Aldrich), anti-β5t antibody (MBL International) (20), anti-β5i antibody (Proteintech) (46), anti-α4s antibody (Proteintech) (22), anti-α6 antibody (Bethyl Laboratories), or anti-β-actin antibody (Cell Signaling Technology) (47), and then with secondary antibodies conjugated to horseradish peroxidase (Santa Cruz). Signals were detected with ECL reagent (GE Healthcare) and Image analysis system (Atto).

Flow cytometric analysis

For the analysis of TECs, minced thymus were digested with 0.5 unit/ml of Liberase (Roche Applied Science) in the presence of 0.02% DNase I (Roche). Single-cell suspensions were stained with antibodies specific for EpCAM (CD326, BioLegend, clone

G8.8), CD45 (BioLegend, clone 30-F11), and Ly51 (CD249, BioLegend, clone 6C3), and for the reactivity with UEA1 (Vector Laboratories). For the analysis of thymocytes and spleen cells, cells were stained with antibodies specific for CD3 (BioLegend, clone 145-2C11), CD4 (BioLegend, clone RM4-5), CD8α (Invitrogen, clone 5H10), TCRβ (BioLegend, clone H57), CD25 (BioLegend, clone PC61), CD44 (eBioscience, clone IM7), and CD69 (eBioscience, clone H1.2F3). Multicolor flow cytometry was performed on FACSVerse.

Proteasome activity assay

Surface-stained thymus cells, testicular cells, and sperm were incubated with 1 μM cell-permeable triple-leucine substrate-based fluorescent probe (Me₄BodipyFL-Ahx₃Leu₃ VS, Boston Biochem), which shows high affinity binding to the chymotrypsin-like catalytic site of proteasomes, at 37 °C for 60 min, and then washed with FACS buffer. Where indicated, the cells were incubated at 37 °C for 1 h in the presence of the proteasome inhibitor MG132 (AdooQ Bioscience) prior to the incubation with the proteasome activity probe. Proteasome activity was measured by flow cytometry.

Tissue analysis

Frozen thymus, testis, and epididymis embedded in OCT compound (Sakura Finetek) were sliced into 10-μm-thick sections. Tissue sections stained with hematoxylin and eosin were examined under a light microscope. For immunofluorescence analysis, the thymus and the testis were fixed in 4% (g/volume) paraformaldehyde and embedded in OCT compound. Frozen tissues were sliced into 10-μm-thick sections. The thymic sections were stained with anti-β5t antibody, anti-Ly51 antibody, anti-Aire antibody, and UEA-1, followed by Alexa Fluor-conjugated secondary reagents. The testis sections were stained with DAPI. Images were analyzed under a TCS SP8 confocal laser-scanning microscope (Leica).

In vitro fertilization assay

Sperm were placed in 1 drop of TYH medium, covered with paraffin oil (Nacalai Tesque), and incubated at 37 °C for 2 h. Eight-week-old C57BL/6 female mice were injected with 5 units of pregnant mare serum gonadotropin 62 h before *in vitro* fertilization and with 5 units of human chorionic gonadotropin 14 h before *in vitro* fertilization. Eggs were collected from the oviduct. In some cases, eggs were treated with 330 g/ml of hyaluronidase (Sigma-Aldrich) or 1 mg/ml of collagenase (Sigma-Aldrich) at 37 °C for 10 min to prepare cumulus-free or zona-free eggs, respectively. The eggs were placed in 1 drop of TYH medium. The eggs were incubated with 2.0 × 10⁵ sperm for 6 h at 37 °C, washed with TYH medium, further incubated for 18 h, and observed under a Hoffman modulation contrast microscope (IX71; Olympus).

Sperm motility assay

To assess sperm motility, sperm in the TYH medium at 37 °C were allowed to swim out from the cauda epididymis for 10 or 120 min and were placed on standard count 2-chamber slides (Leja) (depth 100 μm) that had been preheated to 37 °C. Sperm motility parameters (VCL, VSL, and VAP) were evaluated by a

PITHD1 is essential for male fertilization

computer-assisted system (CEROS II sperm analysis system, software version 1.5.2; Hamilton Thorne Biosciences).

Proteomics analysis

Sperm isolated from PITHD1^{+/+} mice and PITHD1^{-/-} mice in triplicate were lysed in 150 μ l of 6 M guanidine HCl containing 100 mM Tris-HCl, pH 8.0, and 2 mM DTT. The lysates were dissolved by heating and sonication, followed by centrifugation at 20,000 \times g for 15 min at 4 °C. The supernatants containing 100 μ g of protein each were reduced in 5 mM DTT at room temperature for 30 min and alkylated in 27.5 mM iodoacetamide at room temperature for 30 min in the dark. Proteins were purified by methanol/chloroform precipitation and solubilized with 25 μ l of 0.1% RapiGest SF (Waters) in 50 mM triethylammonium bicarbonate buffer. After repeated sonication and vortexing, the proteins were digested with 1 μ g of trypsin/Lys-C mix (Promega) for 16 h at 37 °C. Peptide concentration was determined using Pierce Quantitative Colorimetric Peptide Assay (Thermo Fisher). Approximately 25 μ g of peptides for each sample was labeled with 0.2 mg of TMT6plex reagents (Thermo Fisher) for 1 h at room temperature. After the reaction was quenched with hydroxylamine, all the TMT-labeled samples were pooled, acidified with trifluoroacetic acid (TFA), and fractionated using a Pierce High pH Reversed Phase Peptide Fractionation Kit (Thermo Fisher). Nine fractions were collected using 5, 10, 12.5, 15, 17.5, 20, 22.5, 25, and 50% acetonitrile (ACN) in 0.1% triethylamine. Each fraction was evaporated in a SpeedVac concentrator and dissolved in 0.1% TFA.

LC-MS/MS analysis of the resultant peptides (1 μ g each) was performed on an EASY-nLC 1200 UHPLC connected to a Q-Exactive Plus mass spectrometer through a nanoelectrospray ion source (Thermo Fisher). The peptides were separated on a 75- μ m inner diameter \times 150-mm C18 reversed-phase column (Nikkyo Technos) with a linear gradient of 4–20% ACN for 0–180 min and 20–32% ACN for 180–220 min, followed by an increase to 80% ACN for 220–230 min. The mass spectrometer was operated in the data-dependent acquisition mode with a top 15 MS/MS method. MS1 spectra were measured at the resolution of 70,000, the automatic gain control target of 3×10^6 , and a mass range of 375 to 1,400 m/z . HCD MS/MS spectra were acquired at the resolution of 35,000, the automatic gain control target of 1×10^5 , the isolation window of 0.4 m/z , the maximum injection time of 100 ms, and the normalized collision energy of 32. Dynamic exclusion was set to 30 s. Raw data were directly analyzed against Swiss-Prot database version 2017-10-25 restricted to *Mus musculus* (25,097 sequences) using Proteome Discoverer version 2.2 (Thermo Fisher) with Mascot search engine version 2.5 (Matrix Science) for identification and TMT quantification. The search parameters were (a) trypsin as an enzyme with up to two missed cleavages, (b) precursor mass tolerance of 10 ppm, (c) fragment mass tolerance of 0.02 Da, (d) TMT of lysine and peptide N terminus and carbamidomethylation of cysteine as fixed modifications, and (e) acetylation of protein N terminus and oxidation of methionine as variable modifications. Quantification was performed by using the Reporter Ion Quantification node of the Proteome Discoverer software. Peptides and

proteins were filtered at the FDR of 1% using the percolator node and the protein FDR validator node, respectively.

Statistical analysis

Statistical significance was assessed using the two-tailed unpaired Student's *t* test with Welch's correction for unequal variances. *Q* value was calculated using the multiple unpaired *t* test with the false discovery rate approach (48). The data are presented as mean \pm S.E. of at least three independent experiments.

Data availability

MS proteomics data have been deposited to the ProteomeXchange Consortium via jPOST partner repository with the dataset identifier PXD015347 (49).

Author contributions—H. Kondo, T. M., and I. O. validation; H. Kondo, T. M., M. K., K. I., H. Kosako, and I. O. investigation; H. Kondo, T. M., and I. O. visualization; H. Kondo, T. M., M. I., Y. T., and I. O. writing—original draft; H. Kosako data curation; M. I., Y. T., and I. O. conceptualization; M. I., Y. T., and I. O. supervision; Y. T. and I. O. funding acquisition; Y. T. and I. O. project administration.

Acknowledgments—We thank Drs. Keiji Tanaka, Shigeo Murata, Georg Holländer, Saulius Zuklys, and Sayumi Fujimori for reading the manuscript. We also thank Hitomi Kyuma and Megumi Kawano for technical assistance.

References

1. Coux, O., Tanaka, K., and Goldberg, A. L. (1996) Structure and functions of the 20S and 26S proteasome. *Annu. Rev. Biochem.* **65**, 801–847 [CrossRef Medline](#)
2. Dikic, I. (2017) Proteasomal and autophagic degradation systems. *Annu. Rev. Biochem.* **86**, 193–224 [CrossRef Medline](#)
3. Collins, G. A., and Goldberg, A. L. (2017) The logic of the 26S proteasome. *Cell* **169**, 792–806 [CrossRef Medline](#)
4. Baumeister, W., Walz, J., Zühl, F., and Seemüller, E. (1998) The proteasome: paradigm of a self-compartmentalizing protease. *Cell* **92**, 367–380 [CrossRef Medline](#)
5. Tanaka, K. (2009) The proteasome: overview of structure and functions. *Proc. Jpn. Acad. Ser. B Phys. Biol. Sci.* **85**, 12–36 [CrossRef Medline](#)
6. Murata, S., Yashiroda, H., and Tanaka, K. (2009) Molecular mechanisms of proteasome assembly. *Nat. Rev. Mol. Cell Biol.* **10**, 104–115 [CrossRef Medline](#)
7. Tanaka, K., and Kasahara, M. (1998) The MHC class I ligand-generating system: roles of immuno-proteasomes and the interferon- γ -inducible proteasome activator PA28. *Immunol. Rev.* **163**, 161–176 [CrossRef Medline](#)
8. Fehling, H. J., Swat, W., Laplace, C., Kühn, R., Rajewsky, K., Müller, U., and von Boehmer, H. (1994) MHC class I expression in mice lacking the proteasome subunit LMP-7. *Science* **265**, 1234–1237 [CrossRef Medline](#)
9. Murata, S., Sasaki, K., Kishimoto, T., Niwa, S., Hayashi, H., Takahama, Y., and Tanaka, K. (2007) Regulation of CD8⁺ T cell development by thymus-specific proteasomes. *Science* **316**, 1349–1353 [CrossRef Medline](#)
10. Murata, S., Takahama, Y., Kasahara, M., and Tanaka, K. (2018) The immunoproteasome and thymoproteasome: functions, evolution and human disease. *Nat. Immunol.* **19**, 923–931 [CrossRef Medline](#)
11. Nitta, T., Murata, S., Sasaki, K., Fujii, H., Ripen, A. M., Ishimaru, N., Koyasu, S., Tanaka, K., and Takahama, Y. (2010) Thymoproteasome shapes immunocompetent repertoire of CD8⁺ T cells. *Immunity* **32**, 29–40 [CrossRef Medline](#)

12. Takada, K., Van Laethem, F., Xing, Y., Akane, K., Suzuki, H., Murata, S., Tanaka, K., Jameson, S. C., Singer, A., and Takahama, Y. (2015) TCR affinity for thymoproteasome-dependent positively selecting peptides conditions antigen responsiveness in CD8 (+) T cells. *Nat. Immunol.* **16**, 1069–1076 [CrossRef Medline](#)
13. Livneh, I., Cohen-Kaplan, V., Cohen-Rosenzweig, C., Avni, N., and Ciechanover, A. (2016) The life cycle of the 26S proteasome: from birth, through regulation and function, and onto its death. *Cell Res.* **26**, 869–885 [CrossRef Medline](#)
14. Tanaka, K., Mizushima, T., and Saeki, Y. (2012) The proteasome: molecular machinery and pathophysiological roles. *Biol. Chem.* **393**, 217–234 [CrossRef Medline](#)
15. Schmidt, M., Hanna, J., Elsasser, S., and Finley, D. (2005) Proteasome-associated proteins: regulation of a proteolytic machine. *Biol. Chem.* **386**, 725–737 [Medline](#)
16. Zaiss, D. M., Standera, S., Holzhütter, H., Kloetzel, P., and Sijts, A. J. (1999) The proteasome inhibitor PI31 competes with PA28 for binding to 20S proteasomes. *FEBS Lett.* **457**, 333–338 [CrossRef Medline](#)
17. Andersen, K. M., Madsen, L., Prag, S., Johnsen, A. H., Semple, C. A., Hendil, K. B., and Hartmann-Petersen, R. (2009) Thioredoxin Txn1/TRP32 is a redox-active cofactor of the 26 S proteasome. *J. Biol. Chem.* **284**, 15246–15254 [CrossRef Medline](#)
18. Lu, B., Sun, X., Chen, Y., Jin, Q., Liang, Q., Liu, S., Li, Y., Zhou, Y., Li, W., and Huang, Z. (2015) Novel function of PITH domain-containing 1 as an activator of internal ribosomal entry site to enhance RUNX1 expression and promote megakaryocyte differentiation. *Cell. Mol. Life. Sci.* **72**, 821–832 [CrossRef Medline](#)
19. Kuvardina, O. N., Herglotz, J., Kolodziej, S., Kohrs, N., Herkt, S., Wojcik, B., Oellerich, T., Corso, J., Behrens, K., Kumar, A., Hussong, H., Urlaub, H., Koch, J., Serve, H., Bonig, H., Stocking, C., Rieger, M. A., and Lausen, J. (2015) RUNX1 represses the erythroid gene expression program during megakaryocytic differentiation. *Blood* **125**, 3570–3579 [CrossRef Medline](#)
20. Ohigashi, I., Tanaka, Y., Kondo, K., Fujimori, S., Kondo, H., Palin, A. C., Hoffmann, V., Kozai, M., Matsushita, Y., Uda, S., Motosugi, R., Hamazaki, J., Kubota, H., Murata, S., Tanaka, K., Katagiri, T., Kosako, H., and Takahama, Y. (2019) Trans-omics impact of thymoproteasome in cortical thymic epithelial cells. *Cell Rep.* **29**, 2901–2916.e6 [CrossRef Medline](#)
21. Uechi, H., Hamazaki, J., and Murata, S. (2014) Characterization of the testis-specific proteasome subunit $\alpha 4$ s in mammals. *J. Biol. Chem.* **289**, 12365–12374 [CrossRef Medline](#)
22. Zhang, Q., Ji, S. Y., Busayavalasa, K., Shao, J., and Yu, C. (2019) Meiosis I progression in spermatogenesis requires a type of testis-specific 20S core proteasome. *Nat. Commun.* **10**, 3387 [CrossRef Medline](#)
23. Gómez-H, L., Felipe-Medina, N., Condezo, Y. B., García-Valiente, R., Ramos, I., Suja, J. A., Barbero, J. L., Roig, I., Sánchez-Martín, M., de Rooij, D. G., Llano, E., and Pendas, A. M. (2019) The PSMA8 subunit of the spermatoproteasome is essential for proper meiotic exit and mouse fertility. *PLoS Genet.* **15**, e1008316 [CrossRef Medline](#)
24. Föhse, L., Reinhardt, A., Oberdörfer, L., Schmitz, S., Förster, R., Malissen, B., and Prinz, I. (2013) Differential postselection proliferation dynamics of $\alpha\beta$ T cells, Foxp3+ regulatory T cells, and invariant NKT cells monitored by genetic pulse labeling. *J. Immunol.* **191**, 2384–2392 [CrossRef Medline](#)
25. Berkers, C. R., van Leeuwen, F. W., Groothuis, T. A., Peperzak, V., van Tilburg, E. W., Borst, J., Neefjes, J. J., and Ovaa, H. (2007) Profiling proteasome activity in tissue with fluorescent probes. *Mol. Pharm.* **4**, 739–748 [CrossRef Medline](#)
26. Fujihara, Y., Tokuhira, K., Muro, Y., Kondoh, G., Araki, Y., Ikawa, M., and Okabe, M. (2013) Expression of TEX101, regulated by ACE, is essential for the production of fertile mouse spermatozoa. *Proc. Natl. Acad. Sci. U.S.A.* **110**, 8111–8116 [CrossRef Medline](#)
27. Hagaman, J. R., Moyer, J. S., Bachman, E. S., Sibony, M., Magyar, P. L., Welch, J. E., Smithies, O., Kregge, J. H., and O'Brien, D. A. (1998) Angiotensin-converting enzyme and male fertility. *Proc. Natl. Acad. Sci. U.S.A.* **95**, 2552–2557 [CrossRef Medline](#)
28. Li, W., Guo, X. J., Teng, F., Hou, X. J., Lv, Z., Zhou, S. Y., Bi, Y., Wan, H. F., Feng, C. J., Yuan, Y., Zhao, X. Y., Wang, L., Sha, J. H., and Zhou, Q. (2013) Tex101 is essential for male fertility by affecting sperm migration into the oviduct in mice. *J. Mol. Cell Biol.* **5**, 345–347 [CrossRef Medline](#)
29. Burton, K. A., McDermott, D. A., Wilkes, D., Poulsen, M. N., Nolan, M. A., Goldstein, M., Basson, C. T., and McKnight, G. S. (2006) Haploinsufficiency at the protein kinase A R1 α gene locus leads to fertility defects in male mice and men. *Mol. Endocrinol.* **20**, 2504–2513 [CrossRef Medline](#)
30. Ayaz, A., Agarwal, A., Sharma, R., Kothandaraman, N., Cakar, Z., and Sikka, S. (2018) Proteomic analysis of sperm proteins in infertile men with high levels of reactive oxygen species. *Andrologia* **50**, e13015 [CrossRef Medline](#)
31. Bonache, S., Mata, A., Ramos, M. D., Bassas, L., and Larriba, S. (2012) Sperm gene expression profile is related to pregnancy rate after insemination and is predictive of low fecundity in normozoospermic men. *Hum. Reprod.* **27**, 1556–1567 [CrossRef Medline](#)
32. Kohno, N., Yamagata, K., Yamada, S., Kashiwabara, S., Sakai, Y., and Baba, T. (1998) Two novel testicular serine proteases, TESP1 and TESP2, are present in the mouse sperm acrosome. *Biochem. Biophys. Res. Commun.* **245**, 658–665 [CrossRef Medline](#)
33. Panner Selvam, M. K., Agarwal, A., Pushparaj, P. N., Baskaran, S., and Bendou, H. (2019) Sperm proteome analysis and identification of fertility-associated biomarkers in unexplained male infertility. *Genes* **10**, E522 [Medline](#)
34. Kerns, K., Morales, P., and Sutovsky, P. (2016) Regulation of sperm capacitation by the 26S proteasome: An emerging new paradigm in spermatology. *Biol. Reprod.* **94**, 117 [Medline](#)
35. Ustrell, V., Hoffman, L., Pratt, G., and Rechsteiner, M. (2002) PA200, a nuclear proteasome activator involved in DNA repair. *EMBO J.* **21**, 3516–3525 [CrossRef Medline](#)
36. Qian, M. X., Pang, Y., Liu, C. H., Haratake, K., Du, B. Y., Ji, D. Y., Wang, G. F., Zhu, Q. Q., Song, W., Yu, Y., Zhang, X. X., Huang, H. T., Miao, S., Chen, L. B., Zhang, Z. H., et al. (2013) Acetylation-mediated proteasomal degradation of core histones during DNA repair and spermatogenesis. *Cell* **153**, 1012–1024 [CrossRef Medline](#)
37. Khor, B., Bredemeyer, A. L., Huang, C. Y., Turnbull, I. R., Evans, R., Maggii, L. B., Jr., White, J. M., Walker, L. M., Carnes, K., Hess, R. A., and Sleekman, B. P. (2006) Proteasome activator PA200 is required for normal spermatogenesis. *Mol. Cell Biol.* **26**, 2999–3007 [Medline](#)
38. Yu, G., Zhao, Y., He, J., Lonard, D. M., Mao, C. A., Wang, G., Li, M., and Li, X. (2010) Comparative analysis of REGγ expression in mouse and human tissues. *J. Mol. Cell Biol.* **2**, 192–198 [CrossRef Medline](#)
39. Gao, X., Chen, H., Liu, J., Shen, S., Wang, Q., Clement, T. M., Deskin, B. J., Chen, C., Zhao, D., Wang, L., Guo, L., Ma, X., Zhang, B., Xu, Y., Li, X., and Li, L. (2019) The REGγ-proteasome regulates spermatogenesis partially by P53-PLZF signaling. *Stem Cell Rep.* **13**, 559–571 [CrossRef Medline](#)
40. Huang, L., Haratake, K., Miyahara, H., and Chiba, T. (2016) Proteasome activators, PA28γ and PA200, play indispensable roles in male fertility. *Sci. Rep.* **6**, 23171 [CrossRef Medline](#)
41. Inaba, K. (2011) Sperm flagella: comparative and phylogenetic perspectives of protein components. *Mol. Hum. Reprod.* **17**, 524–538 [CrossRef Medline](#)
42. Takahama, Y., Ohigashi, I., Baik, S., and Anderson, G. (2017) Generation of diversity in thymic epithelial cells. *Nat. Rev. Immunol.* **17**, 295–305 [CrossRef Medline](#)
43. Kiyonari, H., Kaneko, M., Abe, S., and Aizawa, S. (2010) Three inhibitors of FGF receptor, ERK, and GSK3 establishes germline-competent embryonic stem cells of C57BL/6N mouse strain with high efficiency and stability. *Genesis* **48**, 317–327 [Medline](#)
44. Mashiko, D., Fujihara, Y., Satouh, Y., Miyata, H., Isotani, A., and Ikawa, M. (2013) Generation of mutant mice by pronuclear injection of a circular plasmid expressing Cas9 and single guided RNA. *Sci. Rep.* **3**, 3355 [CrossRef Medline](#)
45. Abbasi, F., Miyata, H., Shimada, K., Morohoshi, A., Nozawa, K., Matsumura, T., Xu, Z., Pratiwi, P., and Ikawa, M. (2018) RSPH6A is required for sperm flagellum formation and male fertility in mice. *J. Cell Sci.* **131**, jcs221648 [CrossRef Medline](#)

PITHD1 is essential for male fertilization

46. Fan, X., and Zhao, Y. (2019) miR-451a inhibits cancer growth, epithelial-mesenchymal transition and induces apoptosis in papillary thyroid cancer by targeting PSMB8. *J. Cell Mol. Med.* **23**, 8067–8075 [CrossRef](#) [Medline](#)
47. Bowling, S., Di Gregorio, A., Sancho, M., Pozzi, S., Aarts, M., Signore, M., D Schneider, M., Martinez-Barbera, J. P., Gil, J., and Rodríguez, T. A. (2018) P53 and mTOR signalling determine fitness selection through cell competition during early mouse embryonic development. *Nat. Commun.* **9**, 1763 [CrossRef](#) [Medline](#)
48. Benjamini, Y., and Hochberg, Y. (1995) Controlling the false discovery rate: a practical and powerful approach to multiple testing. *J. R. Stat. Soc. B* **57**, 289–300 [CrossRef](#)
49. Okuda, S., Watanabe, Y., Moriya, Y., Kawano, S., Yamamoto, T., Matsumoto, M., Takami, T., Kobayashi, D., Araki, N., Yoshizawa, A. C., Tabata, T., Sugiyama, N., Goto, S., and Ishihama, Y. (2017) jPOSTrepo: an international standard data repository for proteomes. *Nucleic Acids Res.* **45**, D1107–D1111 [CrossRef](#) [Medline](#)